SARS-CoV-2 spike trimer vaccine expressed in *Nicotiana benthamiana* adjuvanted with Alum elicits protective immune responses in mice

Shi-Jian Song[1,†] (iD), Heeyeon Kim[2,†], Eun Young Jang[3,†], Hyungmin Jeon[1], Hai-Ping Diao[1], Md Rezaul Islam Khan[1], Mi-Seon Lee[4], Young Jae Lee[3], Jeong-hyun Nam[3], Seong-Ryeol Kim[2], Young-Jin Kim[1], Eun-Ju Sohn[5], Inhwan Hwang[1,]* (iD) and Jang-Hoon Choi[2,]*

[1]*Department of Life Science, Pohang University of Science and Technology, Pohang, Korea*

[2]*Division of Acute Viral Disease, Center for Emerging Virus Research, National Institute of Infectious Diseases, Korea National Institute of Health, Cheongju, Korea*

[3]*Division of Vaccine Research, Vaccine Research Center, National Institute of Infectious Diseases, Korea National Institute of Health, Cheongju, Korea*

[4]*Division of Infectious Diseases Inspection, Jeju Special Self-Governing Province Institute of Environment Research, Jeju, Korea*

[5]*BioApplications Inc., Pohang Technopark Complex, Pohang, South Korea*

Summary

The ongoing coronavirus disease 2019 (COVID-19) pandemic has spurred rapid development of vaccines as part of the public health response. However, the general strategy used to construct recombinant trimeric severe acute respiratory syndrome coronavirus 2 (SARS-CoV-2) spike (S) proteins in mammalian cells is not completely adaptive to molecular farming. Therefore, we generated several constructs of recombinant S proteins for high expression in *Nicotiana benthamiana*. Intramuscular injection of *N. benthamiana*-expressed S_{ct} vaccine ($NS_{ct}Vac$) into Balb/c mice elicited both humoral and cellular immune responses, and booster doses increased neutralizing antibody titres. In human angiotensin-converting enzyme knock-in mice, two doses of $NS_{ct}Vac$ induced anti-S and neutralizing antibodies, which cross-neutralized Alpha, Beta, Delta and Omicron variants. Survival rates after lethal challenge with SARS-CoV-2 were up to 80%, without significant body weight loss, and viral titres in lung tissue fell rapidly, with no infectious virus detectable at 7-day post-infection. Thus, plant-derived $NS_{ct}Vac$ could be a candidate COVID-19 vaccine.

Introduction

Severe acute respiratory syndrome coronavirus 2 (SARS-CoV-2) is an enveloped virus that contains a single-stranded RNA genome of 29 903 bp, encoding 16 non-structural proteins, eight accessory proteins and four structural proteins (Mittal *et al.*, 2020; Shang *et al.*, 2020; Yan *et al.*, 2020). Coronaviruses infect a wide range of hosts, including humans. The host specificity is determined by the spike (S) protein, a surface glycoprotein that forms trimers. The S protein can be divided into two functional subunits, S1 and S2, which are separated by proteolytic cleavage by furin or furin-like host proteases (Ord *et al.*, 2020; Peacock *et al.*, 2021). Each of these subunits comprises multiple functional domains. The S1 subunit contains the receptor-binding domain (RBD), which is responsible for binding to a specific protein (or receptor) on the surface of the host cell. Thus, the S1 subunit determines host range and cell tropism (Hossain *et al.*, 2022; Yuan *et al.*, 2021). The S2 subunit, which also contains multiple domains (i.e. a fusion peptide and two heptad repeats), undergoes a dramatic conformational change to produce a so-called trimer of hairpins that supports fusion between the viral and host cell membranes, followed by entry of the virus into the host cell (Berger and Schaffitzel, 2020; Jackson *et al.*, 2022; Xia *et al.*, 2020).

During the ongoing global coronavirus disease 2019 (COVID-19) pandemic, the imperative is to prevent the spread of SARS-CoV-2. Thus, development and production of large amounts of vaccines that are effective against SARS-CoV-2 is necessary. Various approaches have been used to develop such vaccines. Currently, several vaccines (including two mRNA-based vaccines: mRNA-1273; Corbett *et al.*, 2020) and BNT162b2 (Vogel *et al.*, 2021) are in use to protect individuals from infection by SARS-CoV-2. These vaccines induce stronger immune responses, with high neutralizing antibody titres than other types of vaccines in most cases (Francis *et al.*, 2022). However, mRNA-based vaccines appear to cause more side effects than conventional vaccines (Castells and Phillips, 2021). There is also a dispute about the potential risk of reverse transcription of mRNA (Aldén *et al.*, 2022; Zhang *et al.*, 2021). The older platforms (such as protein subunit vaccines) are well accepted by authorities and the lay public compared with novel mRNA platforms. Virus-derived vaccines were also introduced in the field (Bos *et al.*, 2020; Watanabe *et al.*, 2021; Wu *et al.*, 2020), although their protective efficacy is slightly less than that of mRNA-based vaccines because they induce weaker immune responses (Francis *et al.*, 2022). Recently, recombinant protein-based vaccines NVX-Cov2373 (Tian *et al.*, 2021), ZF2001 (Ai *et al.*, 2022) and CoVLP (Ward *et al.*, 2021) were introduced into the field. In contrast to mRNA-based vaccines, these recombinant protein-based vaccines have fewer and weaker side effects and are free from concerns about transgenic contamination. However, the disadvantage of protein-based vaccines is that they take a longer time to develop, and

downstream production is more demanding than DNA or RNA-based vaccines.

Here, we aimed to develop and produce new vaccines against SARS-CoV-2 using recombinant proteins produced in *N. benthamiana*. Recombinant proteins for vaccine development can be produced using multiple approaches. Although proteins can be obtained from inactivated/attenuated viruses, this is not easy because virus amplification requires appropriate cell lines and secure facilities for virus production. Instead, recombinant technology can be used to produce proteins using particle genes obtained from a virus. Traditionally, animal cells or bacteria are used to produce recombinant proteins (Brindha and Kuroda, 2022; Esposito *et al.*, 2020; Gobeil *et al.*, 2021; Li *et al.*, 2020). Recently, however, plants have been used for this purpose because they are easy to grow and production can be scaled up (D'Aoust *et al.*, 2010; Royal *et al.*, 2021; Song *et al.*, 2021). Indeed, using influenza as a model virus, plants have proved to be an excellent system for rapid production of large amounts of recombinant proteins for use as vaccine candidates. Indeed, about 100 million doses of recombinant hemagglutinin (HA) protein were prepared from *N. benthamiana* within 6 weeks via *Agrobacterium*-mediated transformation (D'Aoust *et al.*, 2010). Notably, a plant-based VLP vaccine for SARS-Cov-2 was approved by the Canadian government at the beginning of 2022 (Pillet *et al.*, 2022; Ward *et al.*, 2021). The current COVID-19 situation requires rapid, large-scale production of vaccines to meet the global demand. Here, we describe the use of a plant-based system to generate subunit vaccine candidates for use against SARS-CoV-2.

SARS-CoV-2 surface proteins are a good candidate for vaccine development. This is because all individuals that have recovered from COVID-19 generated anti-S1 and anti-RBD antibodies. However, only a small fraction of these antibodies block the binding of the RBD to the human angiotensin-converting enzyme 2 (hACE2 receptor; Chen *et al.*, 2020). The transient and dynamic conformational states of the S protein mean that there is likely a very limited window during which host B cells are exposed to immunogenic epitopes within the RBD (Pallesen *et al.*, 2017). The S protein of SARS-CoV also induces the production of neutralizing antibodies, including antibodies specific for the RBD.

In this study, we used the full-length S protein lacking the C-terminal transmembrane domain (TMD) and cytosolic tail domain (TMD-C) and asked whether it can be used as a vaccine candidate. We provide evidence that the plant-produced near full-length S protein is highly immunogenic in mice and induced production of antibodies that protect against SARS-CoV-2.

Results

Expression and purification of SARS-CoV-2 S protein from *N. benthamiana*

To identify a vaccine candidate for SARS-CoV-2, we decided to take the recombinant vaccine approach. The S protein expressed on the surface of SARS-CoV-2 is an excellent vaccine candidate compared with its subunit domain RBD or S1, since the S trimer exhibited stronger immunogenicity than that of recombinant S1 protein and RBD protein (Liu *et al.*, 2021). Notably, full-length S protein contains conserved T cell epitopes in the S2 domain (Grifoni *et al.*, 2021), which may contribute to conferring a certain degree of protection against variants. However,

production as a recombinant protein is rather challenging due to its large size, trimeric structure, extensive N-glycosylations and structural instability. Therefore, to produce a recombinant S protein in *N. benthamiana*, we considered various aspects such as expression level, trimerization, structural stability, N-glycosylation and production of a prefusion form. First, to increase expression, we designed a full-length S protein lacking the TMD and C-terminal cytosolic tail domain (SΔ(TMD-C)). Then, we compared the trimerization motifs of the Foldon domain (FD) of bacteriophage T4 fibritin with those of mouse Coronin 1A (mCor1). The FD is a common trimer-inducing domain used for the production of various trimeric recombinant proteins in mammalian cells, including HA (Lu *et al.*, 2014; Santiago *et al.*, 2012; Wei *et al.*, 2008) and S proteins (Esposito *et al.*, 2020; Gobeil *et al.*, 2021). mCor1 is used to induce trimerization of HA (Song *et al.*, 2021). The mode of trimerization between the FD and mCor1 is different, from which the FD domain contains a short N-terminal α-helix structure and a longer C-terminal flexible structure while mCor1 is a complete α-helix structure; therefore, their effect on expression of the fusion protein was unknown. To produce S protein with N-glycosylations, we used the leader sequence of Arabidopsis BiP (ER-localized chaperon) to induce localization in the endoplasmic reticulum (ER; Figure 1a). Additionally, five histidine residues (His5) and an HDEL motif (used as a purification tag and ER retention signal, respectively) were added to the C terminus of the FD or mCor1 to yield the final constructs *BiP:SΔ(TMD-C):FD:His5:HDEL* (S_{ft}) and *BiP:SΔ(TMD-C):mCor1:His5:HDEL* (S_{ct}), respectively. First, we produced these proteins in *N. benthamiana* using the transient expression method (Song *et al.*, 2022).

S_{ft} and S_{ct} bands were detected at approximately 180 kD by Western blot analysis using anti-His antibody (Figure 1c). The apparent size of these proteins was larger than the calculated molecular weight, but similar to that reported in recent studies (Cai *et al.*, 2020; Hsieh *et al.*, 2020). This was due to N-glycosylation since S proteins were expressed in the ER. Consistent with this idea, treatment of purified S proteins with PNGase F caused a shift in migration patterns (Figure 3c). The two trimeric forms, S_{ft} and S_{ct}, showed differences in expression level: the amount of S_{ct} was about 1.8-fold higher than that of S_{ft} according to the result of Western blot analysis (Figure 1b). Therefore, we used mCor1 as a trimerization motif in the following experiments. Next, we introduced a 3P mutation (A942P/K986P/V987P) into the S2 subunit of the S_{ct} construct. These three proline substitutions stabilize the S protein and increase expression in mammalian cells (Pallesen *et al.*, 2017; Hsieh *et al.*, 2020). Finally, we mutated the furin cleavage site to QQAQ to maintain the prefusion form. As a result, S_{ct}-3P and S_{ct}-3PQQAQ were expressed at higher levels than S_{ct} (Figure 1b).

Next, we examined conditions that promote higher-level expression of S_{ct}. A previous study showed that treatment with lipoic acid and ascorbic acid (both antioxidants capable of scavenging reactive oxygen species) along with heat shock treatment led to higher expression in *N. benthamiana* (Norkunas *et al.*, 2018; Wang *et al.*, 2004; Zhao *et al.*, 2017). Of these, heat shock treatment for 30 min at 1-day post-infection (dpi) greatly increased expression of S_{ct} (Figure S1A and B), suggesting that chaperones induced by heat shock play a critical role in high-level expression of the S protein in *N. benthamiana*. This result prompted us to examine the effect of chaperones in the ER, that is, does co-expression of ER chaperones lead to higher expression of S_{ct}? A recent study showed that human calreticulin (CRT)

(a)

(b)

(c)

(d)

(e)
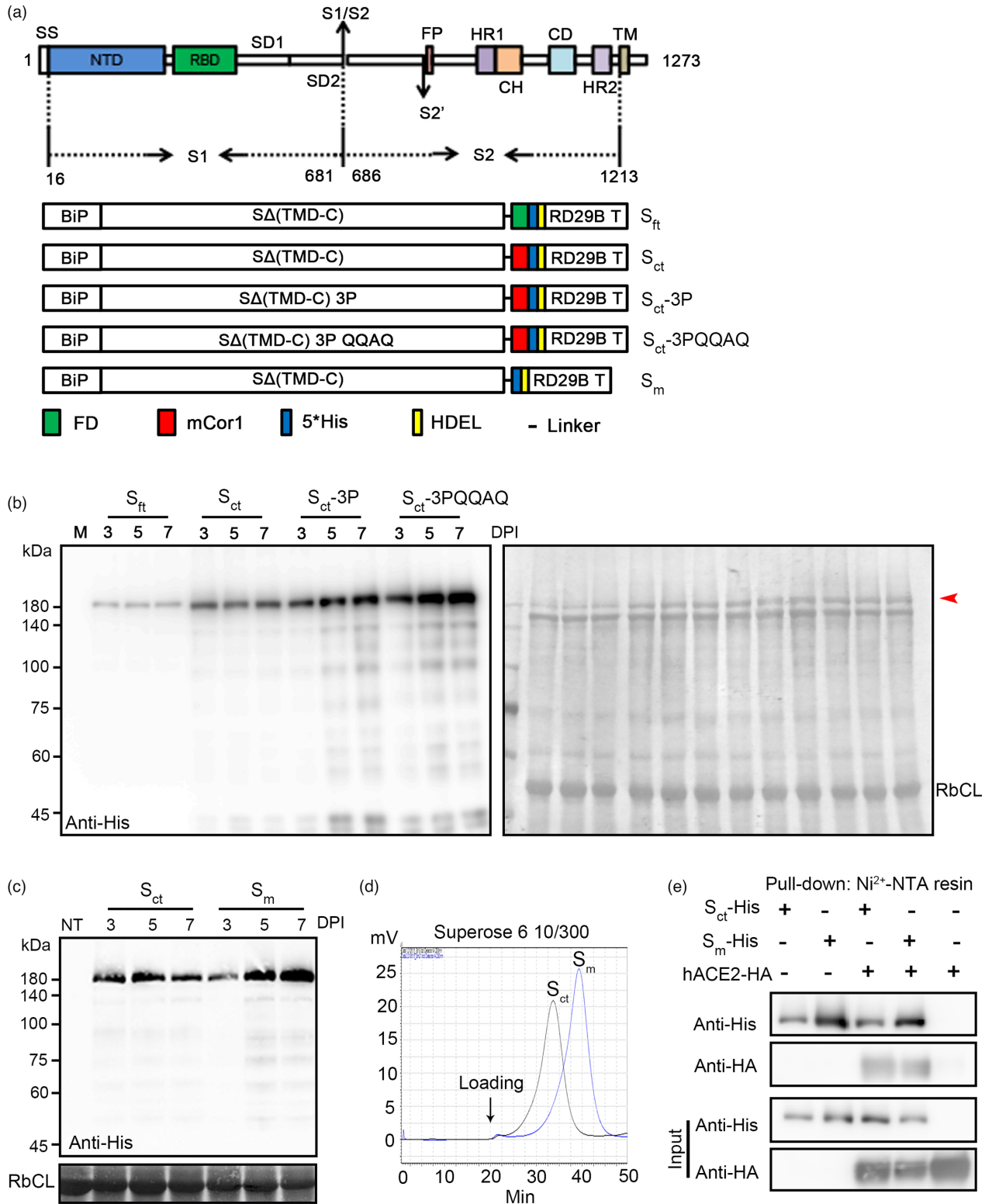
facilitates expression of HIV gp140 in plants (Margolin *et al.*, 2020). We co-infiltrated *N. benthamiana* with a mixture of *Agrobacteria* harbouring S$_{ct}$ and CRT. Indeed, co-expression of CRT increased expression of S$_{ct}$ by 3.51-fold at the ratios of S$_{ct}$ to CRT ranging from 2 : 1 to 5 : 1 (Figure 2a–c). CRT was expressed

at the same level regardless of the ratio, indicating that CRT is highly expressed in *N. benthamiana* (Figure 2b). However, heat shock treatment did not further enhance expression of S$_{ct}$ in the presence of CRT (Figure 2b). Next, we examined the effect of CRT on expression of S$_{ct}$-3P. These results indicate that co-expression

Figure 1 Recombinant S protein produced in *N. benthamiana* binds specifically to hACE2. (a) Schematic representation of the S protein constructs. S (ΔTMD-C), full-length S protein of SARS-CoV-2 (GenBank: MN908947) with deletion of the TMD and the C-terminal region. BiP, the leader sequence of Arabidopsis BiP; FD, Foldon motif; mCor1, the trimerization motif of mouse Coronin 1A; 5*His, 5 histidine residues; HDEL, ER retention signal. Expression of the constructs is under the control of the MacT promoter and the RD29B terminator. (b) Western blot analysis of various S protein constructs. The indicated constructs were transiently expressed in *N. benthamiana* after Agrobacterium-mediated infiltration. Total soluble proteins were prepared from leaf tissues harvested at the indicated DPI and analysed by Western blotting with an anti-His antibody (left), followed by CBB staining of the membrane (right). Red arrow, S proteins. (c) Western blot analysis of S_{ct} and S_m expression. NT, extracts from non-transformed plants. (d) Elution profile of S_{ct} and S_m on a size exclusion column. Proteins purified by Ni^{2+}-NTA affinity column chromatography were subjected to size exclusion chromatography using Superose 6 Increase 10/300. (e) Binding of recombinant S proteins to hACE2. S_{ct} and S_m were co-expressed with hACE2-HA in *N. benthamiana*. Total soluble protein extracts were purified with Ni^{2+}-NTA affinity resin. Proteins eluted from Ni^{2+}-NTA affinity resin were analysed by Western blotting using anti-His and anti-HA antibodies.

of CRT contributes to the folding process of S protein in *N. benthamiana* in a way similar to heat shock treatment (Margolin *et al.*, 2020). However, CRT did not enhance the expression of S_{ct}-3P (Figure 2d), suggesting that the 3P mutation contributes to the folding process which is supported by co-expressed CRT in *N. benthamiana*.

We examined trimerization of S_{ct} at the biochemical level. As a control, we generated a monomeric S protein construct, *BiP:SΔ(TMD-C):His5:HDEL* (S_m) lacking mCor1 (Figure 1a). S_m was expressed at the same level as S_{ct} (Figure 1c). Next, we purified both S_{ct} and S_m by Ni^{2+}-NTA affinity column chromatography. The eluents were further purified by size exclusion chromatography. S_{ct} eluted earlier than S_m at a position corresponding to approximately 600 kD, confirming trimer formation (Figure 1d). To confirm trimerization by mCor1, we generated *BiP:S2Δ(TMD-C):mCor1:His5:HDEL* ($S2_{ct}$) and *BiP:S2Δ(TMD-C):His5:HDEL* ($S2_m$) using the S2 subunit without the TMD and cytosolic domain (Figure S2A). $S2_{ct}$ and $S2_m$ were detected at positions corresponding to 83 and 80 kD, respectively (Figure S2B). Moreover, $S2_{ct}$ also eluted earlier than $S2_m$, consistent with the idea that mCor1 induces trimerization of the S protein (Figure S2C).

As a first step towards vaccine development using S proteins produced in *N. benthamiana*, we used a pull-down assay to examine whether plant-produced S_{ct} and S_m bind to ACE2, the human receptor for SARS-CoV-2. HA-tagged human ACE2 (*hACE2-HA*) was expressed in *N. benthamiana* together with S_{ct} or S_m. Total protein extracts were prepared and pulled down with Ni^{2+}-NTA beads. The pull-down results were analysed by Western blotting using an anti-HA antibody. hACE2-HA was detected in the pull-down from S_{ct} and S_m (Figure 1e), indicating that both S_{ct} and S_m co-expressed in plant cells interact with hACE2.

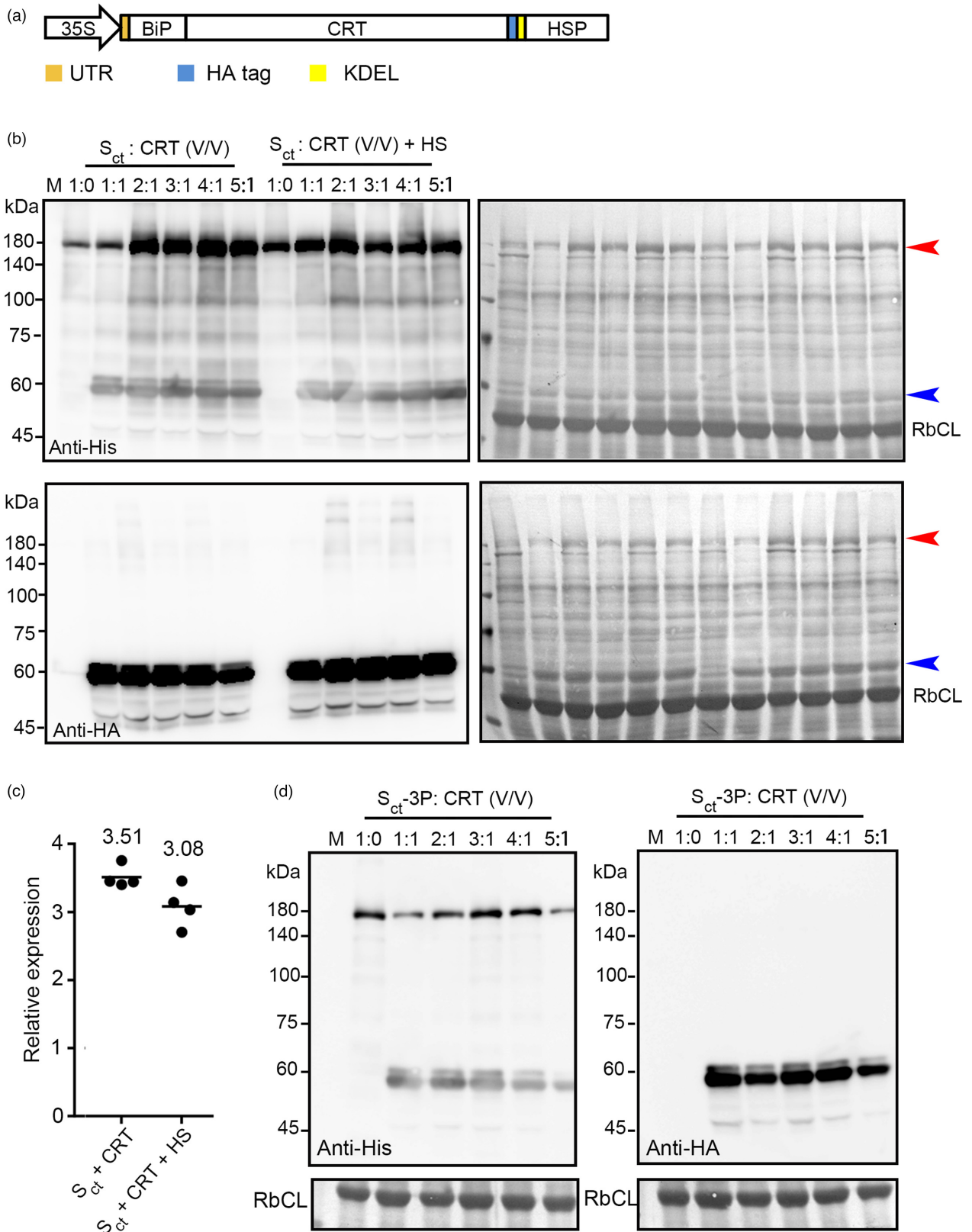## Purification of SARS-CoV-2 S and S2 from *Nicotiana benthamiana*

Next, we optimized the conditions required to purify S_{ct} and $S2_{ct}$ from protein extracts of *N. benthamiana*. First, we purified S_{ct} and $S2_{ct}$ using Ni^{2+}-NTA affinity column chromatography. Here, we first established the purification protocol using total protein extracts prepared from *N. benthamiana* that had been infiltrated with *Agrobacteria* harbouring S_{ct} and *P38*. These proteins contained six histidine residues at the C terminus. Total soluble protein extracts were prepared in TBS buffer (100 mM NaCl, 25 mM Tris–HCl, pH 8, 0.1% Tween 20 and 0.5× protease inhibitor cocktail) and applied to the Ni^{2+}-NTA affinity column. The eluates were subjected to further purification by size exclusion column chromatography. These samples were analysed by SDS-PAGE and stained with CBB. Before and after size exclusion column chromatography, recombinant S_{ct} proteins showed a high degree of aggregation at the top of the separation gel and also

exhibited a smearing background throughout the lane (both with and without DTT; Figure S4A). The amount of high molecular weight aggregates was proportional to the intensity of S_{ct} in the fractions from the size exclusion column (Figure S4B). Moreover, these phenomena were observed for both S_{ct}-3P and S_{ct}-3PQQAQ, despite the fact that the 3P mutation increases the stability of the S protein (Figure S4C), indicating that aggregate formation and smearing may not be caused by instability of the S protein. Plant cells contain high levels of polyphenols, which can bind to proteins and cause smearing (Sęczyk *et al.*, 2019). Thus, to test this idea, leaf tissues ground in liquid nitrogen were mixed with PVPP (Polyvinyl polypyrrolidone) powder and activated carbon (AC) powder, which binds to polyphenols and pigments, and total soluble protein extracts were prepared from the mixture. S_{ct} protein was again purified on an Ni^{2+}-NTA affinity column followed by size exclusion column chromatography. These samples were analysed by SDS-PAGE and stained with CBB (Figure 3a, Figure S4D). S_{ct} proteins from the Ni^{2+}-NTA affinity column did not show high molecular weight aggregation and smearing. Also, the fractions from the size exclusion column no longer aggregated at the top of the separating gel and did not smear throughout the lanes (Figure S4E). After purification, we estimated the yield of purified S_{ct} and found that it was approximately 10 μg per g FW leaf tissue without co-expression of CRT. A significant proportion of S_{ct} did not bind to Ni^{2+}-NTA resin and was found in the flow-through fraction (Figure S3B), indicating that the purification step needs to be further optimized. The yield of purified S_{ct} was rather low without CRT co-expression.

To prepare S_{ct} at a large scale to use for immunization of animals, we expression S_{ct} together with CRT since CRT enhanced the expression level of S_{ct} by 3.51-fold (scale: 1 kg fresh weight of leaf tissue). Upon co-expression of CRT, the expression level of S_{ct} was 106 μg per gram of fresh weight (Figure 2b and Figure S3A). S_{ct} recombinant proteins were purified using Ni^{2+}-NTA affinity column chromatography followed by SEC as established above in Figure 3. Both proteins were diluted to a final concentration of 0.5–0.7 μg/μL (Purity > 95%) for use in animal experiments. Before using S_{ct} for immunization, we also examined the stability of S_{ct}. E-tubes containing 5 μg of purified S_{ct} were kept at 4 °C up to 5 days, which were stored at −80 °C or used for SDS/PAGE analysis. Plant-produced S_{ct} can be stored at 4 °C for 2 days without loss of quality (Figure 3d).

S_{ct} and $S2_{ct}$ produced from *N. benthamiana* form trimers

The behaviour of S_{ct} upon size exclusion chromatography agreed with the expectation of trimer formation. To confirm this, we examined the morphology of the proteins by electron microscopy (EM) after negative staining. S_{ct} and $S2_{ct}$ obtained from a Ni^{2+}-NTA affinity column (Figure 3a, Figure S2D) were further purified

(a)

| 35S | BiP | CRT | | HSP |

■ UTR   ■ HA tag   ■ KDEL

(b)

S_{ct} : CRT (V/V) S_{ct} : CRT (V/V) + HS

M 1:0 1:1 2:1 3:1 4:1 5:1   1:0 1:1 2:1 3:1 4:1 5:1

Anti-His

RbCL

Anti-HA

RbCL

(c)

3.51   3.08

(d)

S_{ct}-3P: CRT (V/V) S_{ct}-3P: CRT (V/V)

M 1:0 1:1 2:1 3:1 4:1 5:1   M 1:0 1:1 2:1 3:1 4:1 5:1

Anti-His

RbCL

Anti-HA

RbCL

by size exclusion chromatography (SEC), the peak fractions were collected, and the proteins were negatively stained. The negative EM images yielded both side and top views of the trimeric S protein particles (Figure 3b, Figure S2E), similar to earlier studies (Cai *et al.*, 2020; Hsieh *et al.*, 2020). These results confirmed that S_{ct} and $S2_{ct}$ are produced as trimers in *N. benthamiana*.

Figure 2 Co-expression of human calreticulin greatly enhances the expression of S_{ct} but not S_{ct}-3P. (a) Schematic representation of the recombinant CRT construct. BiP, the ER targeting leader sequence of Arabidopsis BiP1; CRT, human CRT from aa positions 18–414; HA, the small hemagglutinin tag; KDEL, the ER retention motif; 35S, CaMV 35S promoter; HSP, Arabidopsis HSP terminator. (b, d) Effect of CRT co-expression on S_{ct} or S_{ct}-3P expression. *Agrobacteria* harbouring S_{ct}, S_{ct}-3P, or CRT were cultured in LB medium and resuspended in infiltration buffer at a concentration of OD = 0.8. S_{ct} or S_{ct}-3P-harbouring Agrobacterium resuspensions were mixed with CRT-harbouring Agrobacterium resuspension at ratios from 1 : 0 to 5 : 1 and used for syringe infiltration. Leaf tissues were harvested at 4 DPI, and total soluble protein extracts were prepared for Western blot analysis with anti-His and anti-HA antibodies. Immunoblot membranes were stained with CBB. HS, heat shock treatment by placing the infiltrated plants in a 37 °C incubator for 30 min at 1 DPI. Red arrow, S_{ct}; blue arrow, CRT-HA on CBB-stained PVDF membrane. (c) Quantification of the S_{ct} expression levels upon co-expression of CRT. The signal intensity of S_{ct} upon co-expression of CRT at ratios from 2 : 1 to 5 : 1 was compared with that of S_{ct} alone (1 : 0), with or without heat shock, and presented as relative values.
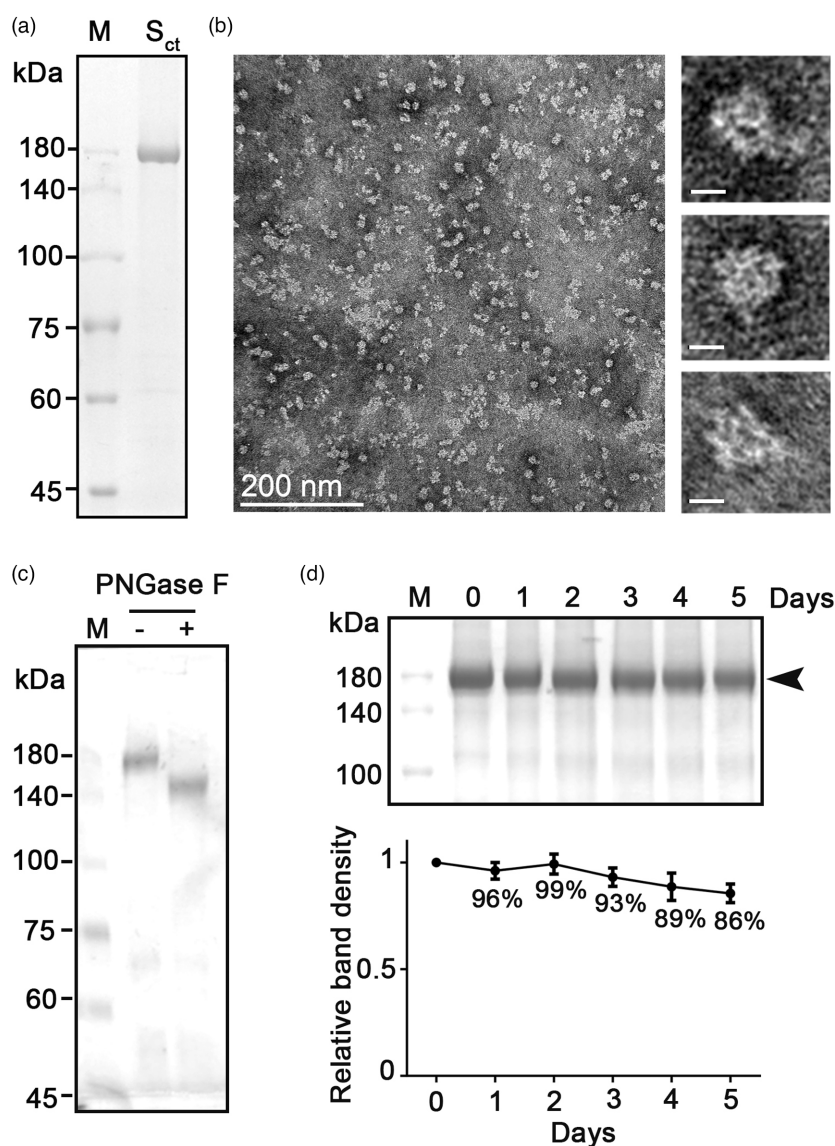
Figure 3 Plant-produced recombinant S_{ct} glycoprotein form trimers. (a) SDS/PAGE analysis of purified proteins. S_{ct} was purified using Ni^{2+}-NTA affinity resin and size exclusion chromatography, and separated by SDS/PAGE, followed by CBB staining. (b) Negative EM analysis of S_{ct}. Scale bars in the magnified pictures indicate 10 nm. (c) Deglycosylation of purified S_{ct}. 2 μg of purified S_{ct} was treated by PNGase F (+) and separated by SDS/PAGE with untreated S_{ct} (−) as a control. (d) Stability of purified S_{ct}. E-tubes containing 5 μg of purified S_{ct} were placed at 4 °C. Samples were taken out on different days and analysed by SDS/PAGE. The band density was quantified. Black arrow indicates the S_{ct}. Statistical analysis was carried out using Student's *t*-test. Error bar, standard error ($n = 3$).
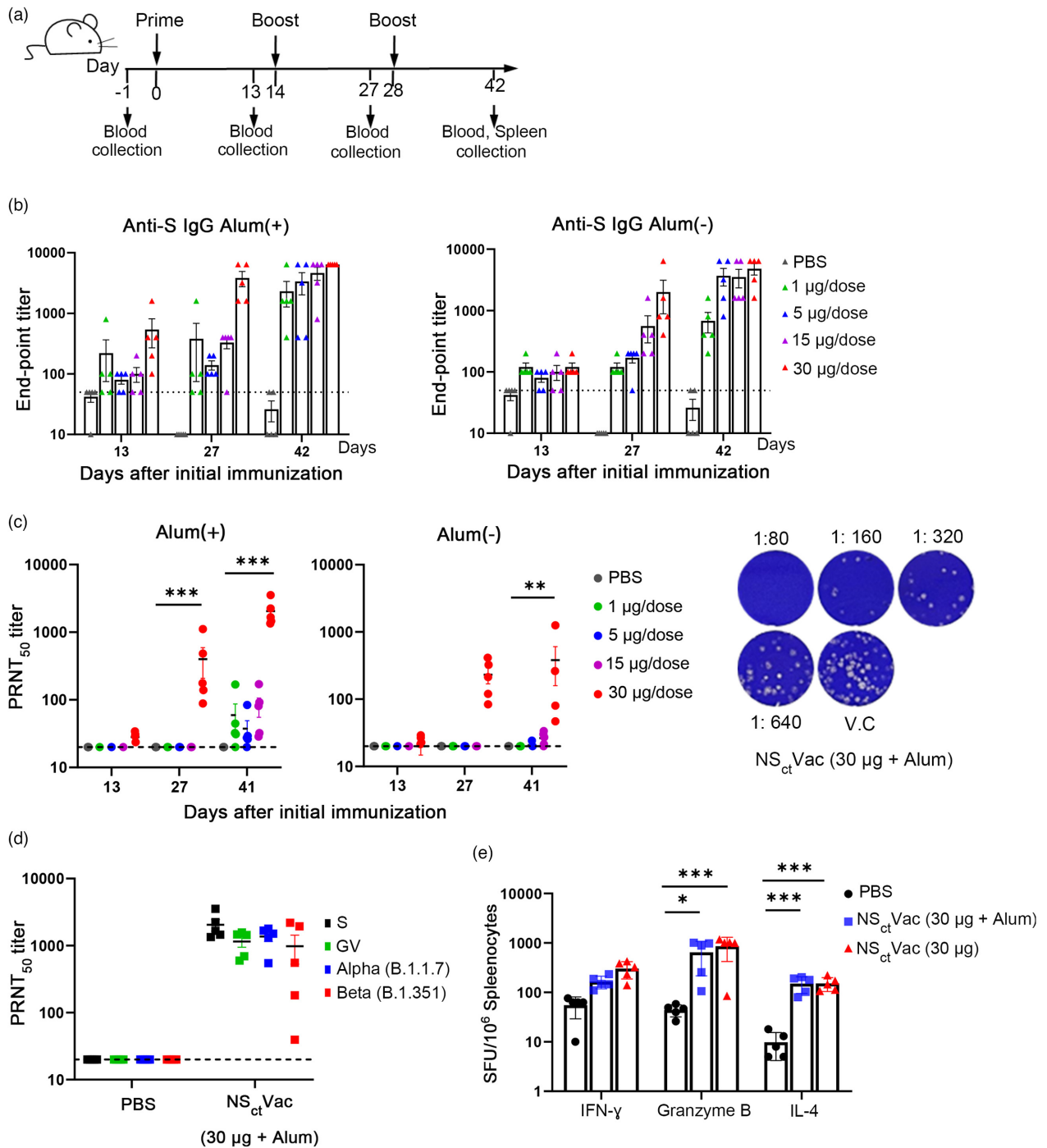
Figure 4 Humoral and cellular immune responses of NS$_{ct}$Vac in mice. (a) Schematic presentation of the mice immunization experiment. Five Balb/c mice per group were injected intramuscularly with NS$_{ct}$Vac, with or without alum hydroxide, and then boosted twice (with an interval of 2 weeks). Mice sera were collected before and after immunization to determine humoral immune responses. (b) The end-point titre of IgG antibodies was tested in ELISA plates coated with recombinant S antigen. (c) The titre of neutralizing antibodies (NAbs) was determined in a 50% plaque reduction neutralizing test (PRNT$_{50}$) at 27 and 42 days post-initial immunization. (d) Cross-neutralizing activity against three variant strains was determined in a PRNT using sera collected at 42-day post-initial immunization. (e) Cytotoxic T cell responses of splenocytes were evaluated 14 days after the 2nd boost. Secretion of IFN-γ and granzyme B was measured in an ELISPOT assay after stimulation with recombinant SARS-CoV-2S protein. Data were expressed as the mean ± SEM. Experiments were conducted independently and in duplicate ($n = 5$ per group/experiment). The statistical significance of differences between groups was calculated by two-way ANOVA with Tukey's multiple comparisons test (*$P < 0.05$, **$P < 0.01$, ***$P < 0.001$). Dotted lines reflect the assay limit of quantitation. See also Figure S3.

NS$_{ct}$Vac induces humoral and cellular immune responses in mice

Immune responses to the *N. benthamiana*-expressed S$_{ct}$ vaccine (NS$_{ct}$Vac) candidate were evaluated in 8-week-old female Balb/c mice ($n = 5$). Mice received an intramuscular injection of various doses (1, 5, 15 and 30 µg) of NS$_{ct}$Vac with or without alum hydroxide as an adjuvant. Mice were boosted twice (with an interval of 2 weeks) after the initial immunization, and sera were collected 1 day before each immunization (Figure 4a). To evaluate S-specific antibodies, we used ELISA plates coated with S protein, the S1 subunit, or the S2 subunit of SARS-CoV-2. On Day 13 post-prime, S antigen-binding antibody responses were detected in mice immunized with low to high doses of NS$_{ct}$Vac. Antibody responses were increased in a dose-dependent manner 2 weeks after the first booster immunization in immunized mice. At 2 weeks after the second boost immunization, antibody levels were elevated in all immunized groups, with the high-dose group (30 µg plus alum hydroxide) reaching saturated end-point titres (Figure 4b). Interestingly, although both S1 and S2 subunit-specific antibodies were induced after the initial immunization, the level of S2-specific antibodies was higher than that of S1-specific antibodies (Figure S5). Moreover, we observed S1- and S2-specific antibody responses after vaccination with inactivated virus, which were comparable with the antibody responses induced by the high dose of NS$_{ct}$Vac. In line with NS$_{ct}$Vac vaccination, we also found that vaccination with inactivated virus elicited higher titres of S2-specific antibodies (Figure S6). In contrast, the placebo group immunized with phosphate saline (PBS) did not produce detectable antibodies.

To determine the neutralizing capacity of sera from immunized mice, we next measured neutralizing antibody (NAb) titres against SARS-CoV-2 S clade strain (KCDC003) in a PRNT assay (we used the same sera used for the ELISAs). After 2 weeks of the first booster shot, neutralizing antibodies were induced only by the high-dose (30 µg) vaccine, with a reciprocal mean titre of ~400 (88–1113). However, after the second booster shot, NAbs were also induced in the low- (1 µg) and medium-dose (5 and 15 µg) groups adjuvanted with alum hydroxide. In the high-dose (30 µg) group, the mean NAb titre reached 2050 (1342–3537), and the deviation between individuals was smaller than in the other groups (Figure 4c). In addition, we evaluated the ability of antibodies elicited by NS$_{ct}$Vac (in mouse sera collected 42-day initial post-immunization) to neutralize the early variant GV (GSAID classification) and two WHO-announced variants of concern (VoC; Alpha, B.1.17 and Beta, B.1.351). Neutralizing titres against these strains were similar to those against the S clade; however, some individuals showed lower titres against the Beta variant than against the prototype S clade strain, although the difference was not statistically significant (Figure 4d).

To evaluate antibody-dependent enhancement (ADE) of infection by S-specific antibodies induced by NS$_{ct}$Vac, we cultured SARS-CoV-2 virus in J774A.1 cells bearing mouse FcγRI/II/III and exposed the cells to serially diluted sera from immunized mice. We then measured the titre of progeny virus in a plaque assay. Since J774A.1 cells can be naturally infected with the SARS-CoV-2 virus, we observed neither virus infection nor ADE (Figure S7).

Cellular immune responses elicited by NS$_{ct}$Vac vaccination were evaluated in an ELISPOT assay with mouse splenocytes. Fourteen days after the second booster, we sacrificed mice and collected splenocytes, which were then cultured with recombinant S antigen as a stimulator. Subsequently, intracellular interferon γ (IFN-γ), granzyme B and interleukin 4 (IL-4) induction were measured. Compared with the placebo group, the NS$_{ct}$Vac-immunized group showed increased secretion of IFN-γ and IL-4. Although IFN-γ was induced to a lesser extent than IL-4, functional granzyme B secretion (indicative of a cytotoxic T cell response) was significantly higher than in the placebo group (Figure 4e).

NS$_{ct}$Vac protects hACE2 transgenic mice from SARS-CoV-2 infection

Finally, we evaluated the protective efficacy of NS$_{ct}$Vac in K18-hACE2 transgenic mice expressing hACE2. Six-week-old K18-ACE2 transgenic mice ($n = 14$) received an intramuscular injection of NS$_{ct}$Vac (30 µg) plus alum hydroxide, followed by a booster 2 weeks later (Figure 5a). Sera were collected 2 weeks after the prime and booster vaccinations and neutralizing antibody production was measured. On Day 13 post-prime, S-specific antibodies were induced in more than half of the mice, reaching a mean titre of 4514 at 13 days after the booster shot (Figure 5b). In addition, S1- and S2-specific antibody responses were similar to those seen in Balb/c mice. NAb titres were elicited after 13-day post-prime, with a mean titre of 76 (35–156), fivefold lower than in Balb/c mice, at 13-day post-boost (Figure 5c). Next, we used mouse sera collected 27-day post-initial immunization to determine the spectrum of cross-neutralization against four recently circulating VoC strains (Alpha, B.1.17; Beta, B.1.351; Delta, B.1.617.2; Omicron, B.1.529). The neutralizing antibody titres were lower than those against the prototype strain (S clade), with mean titres of 30.5, 28.6, 46.9 and 39.8 against Alpha, Beta, Delta and Omicron, respectively. Thus, the titres of Nabs against Delta and Omicron were higher than those against the Alpha and Beta variants (Figure 5d).

Subsequently, we infected NS$_{ct}$Vac-immunized K18-hACE2 mice with 5×10^4 pfu of SARS-CoV-2 (KCDC003) via the intranasal route on Day 14 post-booster injection. Bodyweight changes and survival were observed for 14 days. We found that no significant body weight loss was observed in the vaccinated mice. By contrast, body weight in the placebo control group fell gradually down until Day 8, and only one mouse survived and recovered (Figure 5f). For the purposes of survival analysis, subjects who lost 20% or more of their body weight were considered dead in accordance with the regulation of the Institutional Animal Care and Use Committee of the Korea Centers for Disease Prevention and Control. In the NS$_{ct}$Vac-immunized group, only one mouse was terminated due to body weight loss (on Day 7 post-infection); the remaining mice survived for 2 weeks (a survival rate of 80%). However, four mice in the placebo group succumbed on Day 9 post-infection, and only one survived for 2 weeks (a survival rate of 20%; Figure 5f). To determine the viral titre in lung tissue, three mice were euthanized and tissues were collected at 3-, 5- and 7-day post-challenge. The viral load in the lungs of the NS$_{ct}$Vac-immunized group was lower than that in the placebo group on Day 5 post-challenge. On Day 7 post-infection, no live virus was detected in vaccinated mice, whereas the placebo group still retained virus in the lung tissue (Figure 5e). Histopathological examination of lung tissues showed that SARS-CoV-2 incubation induced extensive inflammation at 3, 5 and 7 post-infection in the placebo group. Whereas, mice immunized with NS$_{ct}$Vac showed minimal lesions (Figure 5g). Taken together, these data suggest that vaccination
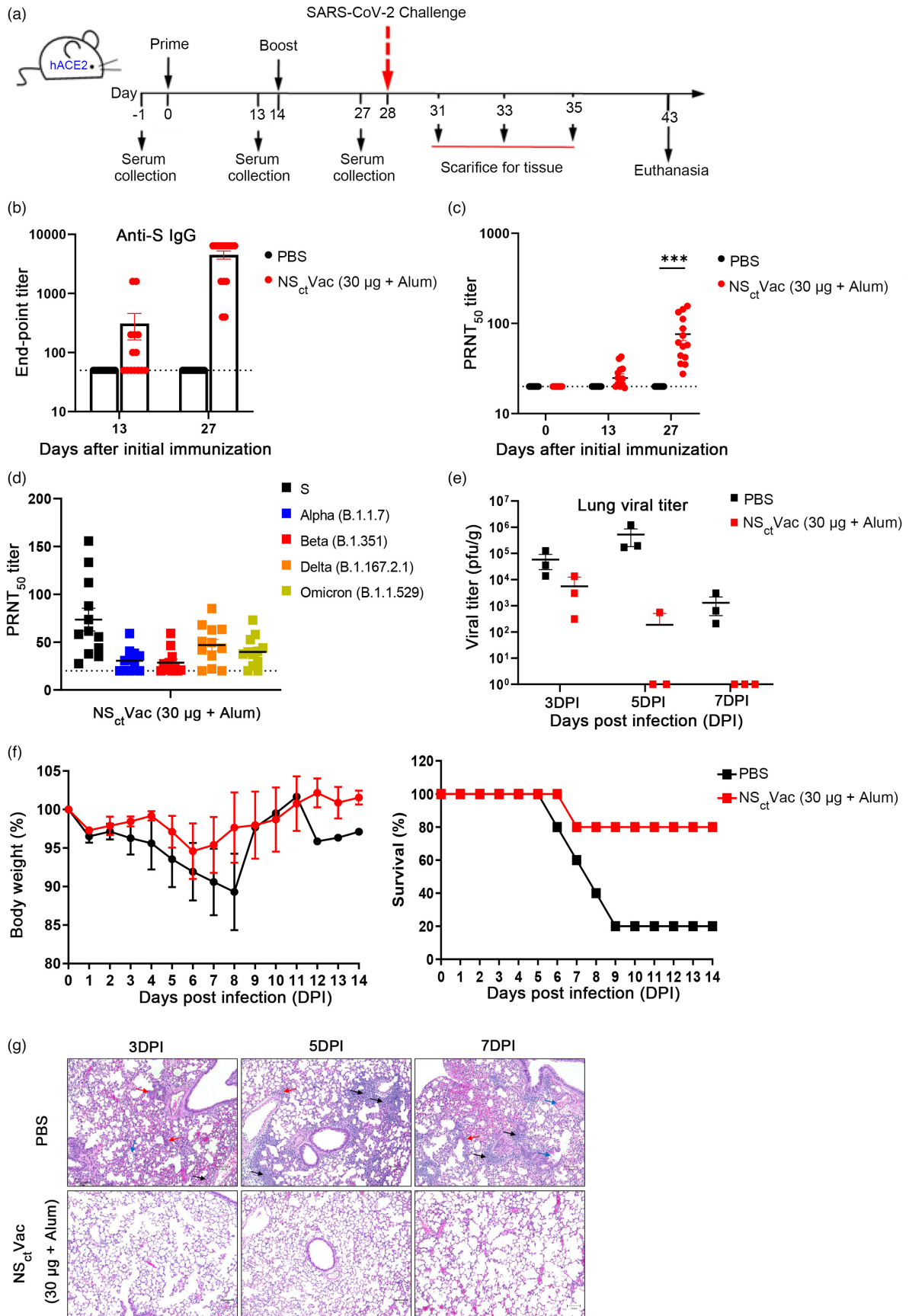
Figure 5 Immunogenicity and protective effects of NS$_{ct}$Vac in hACE2-KI mice. (a) Schematic showing immunization of hACE2 knock-in mice (n = 14) and the viral challenge experiments. Fourteen mice were immunized intramuscularly with NS$_{ct}$Vac with alum hydroxide and then boosted 2-week post-initial immunization. Sera were collected on Days 0, 13 and 27. (b) The end-point titre of IgG antibodies was assessed in ELISAs plates coated with recombinant S antigen. (c) The NAb titre was determined in a PRNT at 13 and 27 days post-initial immunization. (d) Cross-neutralizing activity against four variant strains was determined in a PRNT assay with sera collected at 27-day post-initial immunization (n = 12). (e) At 2-week post-boost, all mice in each group were inoculated intranasally with 5 × 10^4 pfu of SARS-CoV-2 virus (BetaCoV/Korea/KCDC03/2020). After virus challenge, body weight and survival were monitored for 2 weeks (n = 5). (f) Three mice from each group were humanely euthanized on Days 3, 5 and 7 post-infection and the viral titre in the lung was determined in a conventional plaque assay on Vero-E6 cells. (g) Histopathological analysis of lung tissues from virus-inoculated mice. Lung tissues were collected at each time point and sections were stained with haematoxylin and eosin. Black, blue and red arrow indicate neutrophils in the alveolar/interstitial space, proteinaceous debris in air spaces and alveolar septal thickening, respectively. Each image is representative of a group 3 mice. Scale bar: 100 μm, magnification: ×100. Data are expressed as the mean ± SEM. Experiments were conducted independently in duplicate. The statistical significance of the differences between groups was calculated by two-way ANOVA with Tukey's multiple comparisons test (*P < 0.05, **P < 0.01, ***P < 0.001). Dotted lines reflect the assay limit of quantitation.

with NS$_{ct}$Vac induces protection in K18-hACE2 mice challenged with a high dose of virus.

Discussion

Expression level is a key aspect of recombinant protein production. Therefore, we explored various conditions. In general, membrane proteins have limitations with respect to high-level expression. We used a full-length protein lacking the TMD and the C-terminal domain. Another consideration was to produce a trimeric recombinant S protein to mimic that expressed by the native virus. Of the two trimerization motifs, FD and mCor1, we found that mCor1 was better for the expression level. We also examined the effect of double proline substitution (2P) in the S2 subunit that prevents fusogenic conformational change of MERS-CoV S (Pallesen *et al.*, 2017), thereby stabilizing the prefusion state of S glycoproteins, which in turn leads to an increase in the final production yield. 2P substitution was used for the current SARS-CoV-2 vaccines. Moreover, a Hexa proline substitution (6P) increases the final yield in mammalian cells (Hsieh *et al.*, 2020). The 3P substitution in the S2 subunit increased expression of the S protein in *N. benthamiana*. This suggests that the stability of the S protein is important for high-level expression in plants. Consistent with this idea, heat shock treatment and co-expression of CRT greatly enhanced the expression level. However, CRT and 3P did not show any additive effect in plants. Besides, a furin cleavage site mutation from RRAR to QQAQ was included in the subunit vaccine NVX-Cov2373 to prevent cleavage of the S protein into its S1 and S2 subunits. However, S$_{ct}$ expressed in plants was not subjected to cleavage at the furin site. This may be due to localization of the S protein in the ER. Another possibility is that plants may not contain furin homologues since no furin cleavage activity was been observed in plants (Mamedov *et al.*, 2019; Wilbers *et al.*, 2016).

Protein purification, which is thought to account for up to 80% of total production costs (Buyel, 2015; Wilken and Nikolov, 2012), is the most challenging step during recombinant protein production. Initially, we used the same buffer conditions as those for S protein purification from animal cells, but found that they were not suitable for purification of recombinant S$_{ct}$ proteins from *N. benthamiana* extracts. S$_{ct}$ proteins purified from *N. benthamiana* were highly aggregated and exhibited a smeared background on the SDS-PAGE (Figure S4A), which was not removed after gel infiltration (Figure S4B). Plant extracts contain high levels of polyphenolic compounds and pigments, which can

interfere with protein purification by interacting with proteins or binding to the affinity resin. Therefore, we optimized the extraction buffer with respect to the type and concentration of salt, buffer pH and detergents. Upon pretreatment of ground leaf tissues with PVPP and AC, two polyphenol adsorbents that bind to polyphenols and pigments, recombinant S$_{ct}$ protein no longer produced high molecular weight aggregates or a smeared background during purification. PVPP is used to remove polyphenols during beer and juice manufacturing (Cimini *et al.*, 2014; Youn *et al.*, 2004). Polyphenol is a kind of polymer containing several to dozens of –OH groups that bind to proline-rich segments of proteins. Also, polyphenolic compounds can interact with resins such as Ni^{2+}-NTA, thereby interfering with specific binding of the His-tag to the resin. Finally, we set up the purification protocol in such a way that L-proline, PVPP and AC were mixed with ground tissue powder before adding extraction buffer; this eliminated the polyphenolic compounds and pigments.

The immunogenicity and protective efficacy of NS$_{ct}$Vac were evaluated in Balb/c and K18-hACE2 mice. Antibody responses to NS$_{ct}$Vac in mice were comparable with those induced by plant-derived recombinant protein antigen vaccines published by others (Mamedov *et al.*, 2021; Tran *et al.*, 2021). Notably, we found that alum hydroxide adjuvant increased humoral immunity in all vaccinated groups, but not cellular immunity (Figure 4e). These results are consistent with a previous report (Hogenesch, 2012). Since NS$_{ct}$Vac comprises the full-size trimeric S antigen, we performed ELISAs with three different coating antigens to detect S1 and S2 subunit-specific antibodies. Unexpectedly, S2-specific antibodies were induced at relatively high concentrations (Figure S5). Similarly, we found that S2-specific antibody levels in sera from mice infected with inactivated virus were similar to those in vaccinated mice (Figure S6). As such, it is plausible that the intact S antigen elicits a high S2 antibody response, which is consistent with a recent study describing high levels of anti-S2 antibodies in serum from COVID-19 convalescent subjects (Nguyen-Contant *et al.*, 2020). The structurally conserved SARS-CoV-2 S2 subunit shows >88% sequence homology among Beta coronaviruses, including previous SARS-CoVs; therefore, the functional S2 fusion peptide region might confer cross-neutralizing potency against other coronaviruses (Walls *et al.*, 2020). High levels of S2-specific antibodies might have cross-reactive potential as we observed no significant ADE infection in this study (Figure S7).

In line with IgG generation, NAbs were induced 2 weeks after the primary vaccination, and titres increased following the booster

shots (Figure 4c). Due to the limited amount of serum collected from each Balb/c mouse, we only conducted PRNT against the GV (GSAID classification), Alpha (B.1.1.7) and Beta (B.1.351) variants available at that time. Antibody-mediated neutralization activity against the Beta variant was partially reduced; however, there was no significant difference in the neutralizing activity of the other variants (Figure 4d). In addition, neutralizing titres against Delta (B.1.617.2.1) and Omicron (B.1.1.529) were somewhat decreased in K18-hACE2 mice serum after the booster shot (Figure 5d). This finding is consistent with those of recent clinical studies showing that two-dose vaccination with the currently used mRNA vaccines provides limited protection against infection by the Omicron variant (Sarah A. Buchan, 2022). However, a third booster dose of the current mRNA vaccines increases vaccine efficacy and neutralizing antibody titres against the Omicron variant, which may lower the risk of breakthrough infection (Andrews et al., 2022; Nemet et al., 2022; Pajon et al., 2022; Simone I. Richardson et al., 2022). As human CD8^{+} T cell epitopes are located throughout the SARS-CoV-2 S gene (Grifoni et al., 2021), a full-length S recombinant vaccine may stimulate T cell responses to a greater extent than a partial subunit vaccine such as an RBD targeted vaccine. Antigen-specific T cell responses to NS$_{ct}$Vac were determined after *ex vivo* stimulation of splenocytes. The number of IFN-γ- and granzyme B-secreting cells after vaccination was 5- and 15-fold higher, respectively, than in the placebo group, implying cross-presentation of recombinant NS$_{ct}$Vac vaccine to antigen-presenting cells (Heath and Carbone, 2001; Joffre et al., 2012). The protective efficacy of NS$_{ct}$Vac was evaluated by challenging hACE2 knock-in mice, which showed severe illness and mortality after intranasal infection with SARS-CoV-2, with live virus (Oladunni et al., 2020). Despite the finding that NS$_{ct}$Vac-vaccinated K18-hACE2 mice have a weaker antibody response than Balb/c mice, there was a protective effect against challenge infection. As previously described, host T cells provide a complementary protective effect against SARS-CoV-2 infection, particularly when the humoral immune response is insufficient (Zhuang et al., 2021). Thus, T cell immunity contributes to protection from infection and ameliorates disease severity.

Although this study demonstrates the immunogenic and protective effects of a plant-derived vaccine in murine models, there are several limitations. First, although we measured overall IFN-γ secretion in splenocytes by ELISPOT, in-depth analysis of CD4^{+} and CD8^{+} T cell responses should be undertaken to fully identify the protective mechanism. Second, NS$_{ct}$Vac vaccination induced large amounts of S2-specific antibodies; however, the role of these antibodies remains to be addressed. Since the S2 subunit is conserved across coronaviruses (Shah et al., 2021), it is plausible to examine cross-reactivity among coronaviruses. Third, a 2-week vaccination interval may not be optimal. Since insufficient B cell maturation is attributed to a short vaccine interval, high levels of neutralizing antibody induction and affinity maturation may not occur (Rossler et al., 2022).

Regarding the current situation of variants pandemics, SARS-Cov-2 is constantly mutating and breaking through the pre-established immunity. Fast updating and producing the vaccines for new variants economically is crucial for controlling the waves of the pandemic worldwide. Plant-based vaccine manufacturing has various advantages (e.g. rapid production, cost-effectiveness and easy scalability) over mammalian systems; thus, it can be used to rapidly supply cheap vaccines to fight emerging infectious disease pandemics (Dhama et al., 2020). Currently, there have

been several attempts to develop COVID-19 vaccines using plant-derived subunits and VLP platforms (ClinicalTrials.gov, 2022; Maharjan and Choe, 2021; Mamedov et al., 2021; Siriwat-tananon et al., 2021) or plant-derived products to prophylactic protection against COVID-19 in general social settings (Daniell et al., 2022). Of these, a VLP vaccine from Medicago Inc. is the only licensed vaccine to date (HealthCanada, 2022). In all these efforts, one crucial aspect is the yield of proteins produced in *N. benthamiana*. In this study, we used an ordinary binary vector with a strong promoter and terminator and obtained 106 μg/g of fresh weight. For real commercialization, higher levels of expression would be more preferable. In fact, many high-performing vectors based on RNA or DNA viruses have been developed that can be used for commercialization of vaccine produced using S$_{ct}$ in the future.

In summary, immunization with a SARS-CoV-2 S trimer vaccine expressed in *N. benthamiana* induces robust humoral and cellular immune responses in mice, which confer protection against lethal challenge. Immunization with the prefusion-stabilized trimeric S induced broad-spectrum antibodies in a manner similar to natural viral infection. Thus, we suggest that plant-derived vaccines will be a useful platform in the near future and that NS$_{ct}$Vac has potential as another plant vaccine candidate in addition to VLP.

Materials and methods

Cells and viruses

Vero-E6 (CRL-1586) cells were purchased from the American Type Culture Collection (Manassas, VA) and maintained in Dulbecco's modified Eagle's medium (DMEM) supplemented with 10% FBS, 100 U/mL of penicillin and 100 μg/mL of streptomycin (Gibco, NY). The SARS-CoV-2 viruses [BetaCoV/Korea/KCDC03/2020, hCoV-19/Korea/KDCA23857/2020 (GV), hCoV-19/Korea/KDCA51463/2021 (Alpha) and hCoV-19/Korea/KDCA55905/2021 (Beta), hCoV-19/Korea/KDCA119861/2021 (Delta) and hCoV-19/Korea/KDCA447321/2021 (Omicron)] were obtained from the National Culture Collection for Pathogens at the Korea National Institute of Health (KNIH). Viruses were propagated in Vero-E6 cells, and the virus stocks were stored at −70 °C until use. All experiments using viruses, including those in mice, were performed in the animal biosafety level 3 (ABSL-3) laboratory facilities at KNIH.

Design and construction of the SARS-CoV-2 S and S2 vaccine candidates

The ectopic region of the S protein from amino acid positions 16 to 1213 [SΔ(TMD-CT)] was codon-optimized and chemically synthesized (Gene Universal, Newark). *BamH1:SΔ(TMD-CT):L:Spe1* was PCR amplified from template SΔ(TMD-CT) using primers F-S and R-S. *BamH1:S2:Spe1* was PCR amplified from template SΔ(TMD-CT) using primers F-S2 and R-S. The site-specific mutations were introduced by two-step PCRs. The primers used for the A942P mutation were F-S, R-A942P, F-A942P and R-S; those used for the K986P/V987P mutations were F-S, R-K986P/V987P, F-K986P/V987P and R-S; and those used for the QQAQ mutation were F-S and R-QQAQ, F-QQAQ and R-S. The trimerization motifs of the Foldon domain (FD; GYIPEAPRDG-QAYVRKDGEWVLLSTFL) or mouse Coronin 1A (mCor1; VSRLEEDVRNLNAIVQKLQERLDRLEETVQAK), together with additional flanking regions (*Spe1:Linker:FD:His5:HDEL:XhoI* and *Spe1:Linker:mCor1:His5:HDEL:XhoI*, respectively), were chemically

synthesized. The PCR fragment *BamH1:SΔ(TMD-CT):L:Spe1* was ligated to *Spe1:Linker:FD:His5:HDEL:XhoI* or *Spe1:Linker:mCor1:His5:HDEL:XhoI* and ligated downstream of the leader sequence of *Arabidopsis* BiP in the *pTEX1* vector harbouring the *MacT* promoter and the *RD29B* terminator (Song *et al.*, 2021) using restriction endonuclease sites *BamHI* and *XhoI* to give *BiP:SΔ(TMD-CT):FD:His5:HDEL* and *BiP:SΔ(TMD-CT):mCor1:His5:HDEL*, respectively. *SΔ(TMD-CT)* in *BiP:SΔ(TMD-CT):mCor1:His5:HDEL* was replaced with *BamH1:S2:Spe1* to yield *BiP:S2:mCor1:His5: HDEL*. The sequences of the primers are listed in the Table S1.

Expression and purification of recombinant S proteins from *N. benthamiana*

The expression vectors were transformed into *Agrobacterium* strain GV3101 and transiently expressed in 4–5-week-old *N. benthamiana* plant leaves using Agroinfiltration. The infiltrated leaves were harvested at 3-, 5- and 7-day post-infiltration (DPI) to examine expression. To obtain a large amount of infiltrated leaves, the vacuum-mediated Agroinfiltration method was used and plant leaves were harvested at 5 dpi. To examine expression of recombinant S and S2 proteins, infiltrated leaves were ground and mixed with protein extraction buffer (300 mM NaCl, 50 mM Tris–HCl, pH 8.5, 1 mM EDTA, 0.1% Triton X-100 and 1 × protease inhibitor cocktail) at a ratio of 5:1 (V/W). The extracts were separated on 7.5% SDS-PAGE gels and analysed by Western blotting with a mouse anti-His antibody (15 000 dilution). The blot was developed with the enhanced chemiluminescence kit (Amersham Pharmacia Biotech, Piscataway, NJ), and images were captured using the LAS3000 system (Fujifilm, Tokyo, Japan).

To purify recombinant proteins, Ni^{2+}-NTA affinity column chromatography was performed according to the manufacturer's protocol. Briefly, total protein extracts were prepared using 3 volumes of extraction buffer (100 mM NaCl, 25 mM Tris–HCl, pH 8, 2 mM $CaCl_2$, 0.1% Tween 20, 0.5% L-proline, 0.5% AC, 0.5% PVPP and 0.5 × protease inhibitor cocktail). The mixture was shaken for 20 min in a cold room, followed by additional shaking for 10 min after addition of 2 mM Na^+-phytate. The mixture was subjected to centrifugation at 18 000 ***g*** (3 × 10 min), and the supernatant was collected. Total protein extracts were loaded onto an Ni^{2+}-NTA affinity column, followed by washing three times. Proteins were eluted using a total of 15 mL buffer containing 400 mM imidazole. The eluates were concentrated and loaded onto a Superose 6 10/300 increase column or a HiLoad 16/60 Superose 6 pg column and analysed using a fast protein liquid chromatography system (AKTA purifier GE Healthcare systems) at 4 °C in TBS (100 mM NaCl, 25 mM Tris–HCl, pH 8). Proteins were eluted in TBS at a flow rate of 0.4 mL/min per fraction or 1 mL/min per fraction, and the concentration was measured at 280 nm. Fractions from the column were analysed by SDS-PAGE and CBB staining. The fractions containing the majority of the S proteins were collected and concentrated using Centricon filters (Ultracel-30K, Merck, CORK, IRELAND) to yield a final concentration of approximately 0.5–0.7 mg/mL.

Enzymatic deglycosylation of purified S_{ct} proteins

Purified S_{ct} protein was subjected to treatment with PNGase F (NEB #P0710) according to a previous study (Song *et al.*, 2021). Briefly, 2 μg of S_{ct} was denatured by boiling for 10 min. The denatured protein (10 μL) was chilled on ice and mixed with 2 μL GlycoBuffer (10×), 2 μL 10% NP-40, 5 μL H_2O and 1 μL PNGase F and incubated at 37 °C for 1 h. The samples were separated by SDS/PAGE, followed by CBB staining.

Negative staining and EM

Carbon-coated copper grids (Electron Microscopy Sciences) were glow-discharged at 15 mA for 30 s using a Pelco-Easiglow™ glow discharge cleaning system (Ted Pella). Purified S_{ct} and $S2_{ct}$ spike trimer samples (0.01 mg/mL) were loaded on the glow-discharged carbon-coated copper grids for 1 min. Uranyl acetate (30 μg, 2%, wt/vol) was used to stain the samples on the grid for 2 min. The stained grid was then blotted with filter paper, dried and stored for TEM analysis. TEM analysis was performed using a JEOL JEM-1011 TEM (JEOL USA, Inc., Peabody, MA). Images were obtained at a magnification of ×150 000.

Immunization of Balb/c mice

Specific pathogen-free female BALB/c mice aged 6–8 weeks (Orient Bio, Sungnam, Korea) were used to investigate humoral and cellular immune responses. Mice (*n* = 5/group) were immunized with various doses (1, 5, 15 and 30 μg) of *N. benthamiana*-derived trimer S vaccine ($NS_{ct}Vac$) via the intramuscular route, with or without 50 μL of 2% alum hydroxide adjuvant (Alhydro® gel; Invivogen). Two boosters were given post-initial immunization (at an interval of 14 days). Sera were collected at 1 day before each immunization to detect SARS-CoV-2 spike-specific IgG and neutralizing antibodies. Spleens were collected at Day 42 after initial immunization to assess cellular immunity by ELISPOT (R&D Systems, MN). All animal experiments were authorized by the Institutional Animal Care and Use Committee of the Korea Centers for Disease Prevention and Control (Protocol approval No. KCDC-075-19-2A), and all experiments were performed according to the guidelines of this committee.

Human ACE2 knock-in mice immunization and challenge

For the virus challenge experiments, 14 female hACE2 knock-in transgenic mice (B6.Cg-Tg(K18-hACE2)2Prlmn/J; aged 6–8 weeks; Jackson Laboratory, ME) were immunized with $NS_{ct}Vac$ (30 μg) plus alum hydroxide via the intramuscular route. Mice were boosted 2 weeks after the initial immunization. On Day 28 post-priming, mice were anaesthetized by intra-peritoneal injection avertin (200 mg/kg) and inoculated intranasally with 5×10^4 pfu SARS-CoV-2 virus (BetaCoV/Korea/KCDC03/2020). Three mice were euthanized humanly, and lungs were collected to determine the viral load in a plaque assay (Cho *et al.*, 2020) and histopathology on Days 3, 5 and 7 post-infection. The remaining mice (*n* = 5) were monitored continuously for 14 days to assess body weight changes and survival.

Enzyme-linked immunosorbent assay (ELISA)

Recombinant full-length SARS-CoV-2 spike (S), subunit 1 (S1) and subunit 2 (S2) proteins were expressed in *Escherichia coli* (BL21-DE3) and purified using an Ni^{2+}-NTA column (Thermo Fisher). To detect spike-specific antibodies, 96-well plates were coated with purified recombinant S protein (0.5 μg/well) in PBS and incubated at 4°C overnight. After incubation, plates were washed three times with PBST (0.05% Tween 20 in PBS) and blocked with 5% skim milk in PBS. Serially diluted (twofold in blocking buffer, starting at 1 : 50) mouse serum was added to the plates for 1 h at room temperature. After washing with PBST, rabbit anti-mouse IgG-HRP (Southern Biotech, AL; diluted 1 : 1000 in blocking buffer) was added for 1 h. The colour signal was developed using o-phenylenediamine dihydrochloride (OPD) substrate solution (0.5 mg/mL OPD in 0.05 M phosphate citrate buffer, pH 5.0;

Sigma), and the reaction was stopped by adding 100 μL of 0.5 M sulphuric acid. Absorbance at an optical density (OD) of 490 nm was measured using an EPOCH microplate reader (BioTek, VT). Serum titres were determined as the largest reciprocal of the end-point dilution that was greater than twice the background value.

Plaque reduction neutralization assay (PRNT)

Vero-E6 cells (200 000 cells/well) were seeded in 12-well plates and incubated for 16 h until 90% confluent. Serum samples were inactivated at 56 °C for 30 min and serially diluted (twofold diluted, starting at 1 : 10) in DMEM (Gibco) containing 2% FBS (Gibco) and 1% penicillin–streptomycin (P/S; 10 000 U/mL; Gibco). The diluted sera were mixed with the same volume of virus to generate a mixture containing ~80 PFU/200 μL of virus and then incubated at 37 °C for 1 h. The virus-serum mixture was added to Vero-E6 cell monolayers at 37 °C for 1 h. The mixtures were removed, and cells were overlaid with 1% sea plaque agarose (LONZA) in MEM (Gibco) containing 2% FBS and 1% P/S. After further incubation at 37 °C for 3 days, the plates were fixed with 4% paraformaldehyde (Biosesang, Korea) and stained with 1% crystal violet (Sigma-Aldrich, St. Louis, MO, USA). The 50% neutralization titre ($PRNT_{50}$) was calculated using the Reed and Muench method (Reed and Muench, 1938).

Enzyme-linked immunosorbent spot assay (ELISPOT)

On Day 14 after the second boost, Balb/c mice spleens were isolated and the tissues were ground and filtered through a 70 μm nylon mesh cell strainer (Corning) to yield splenocytes. After red blood cells (RBC) were lysed using RBC lysis buffer, assays were performed using ELISpot kits (R&D Systems). Briefly, monoclonal antibodies specific for mouse IFN-γ, IL-4 or Granzyme B were pre-coated onto a PVDF-backed microplate and blocked with blocking buffer (10% FBS in RPMI). Splenocytes (1×10^6) were seeded into each well and stimulated with either DMSO (negative control) or 2 μg/mL recombinant S protein of SARS-CoV-2 (Sino Biological Inc., China). After incubation for 48 h at 37 °C/5% CO_2, biotinylated anti-mouse IFN-γ, IL-4 or Granzyme B antibodies were added to each well at room temperature for 2 h. Finally, the spots were developed using a BCIP/NBT substrate. The number of spot-forming cells on the plates was counted using an automated CTL Analyzer system (Cellular Technology, Cleveland, OH).

ADE assay

The murine monocyte–macrophage cell line (J774A.1) was seeded in 24-well plates at a density of 1.5×10^5 cells per well. Serially diluted mice sera were mixed with SARS-CoV-2 virus at a multiplicity of infection of 0.01 and incubated for 1 h. The virus/serum mixtures were added to the cells and incubated at 37 °C for 48 h. Cells and supernatants were harvested by centrifugation at 200 *g* for 5 min, and the virus titre in Vero-E6 cells was measured by plaque assay.

Statistical analysis

Details regarding statistical analysis are provided in the figure legends. The end-point IgG titre is presented as the mean titre along with the standard error of the mean (SEM) and was calculated by assigning a titre of 10 to samples with no detectable IgG antibodies at the starting dilution (titre <50). The statistical significance of differences between control and vaccination groups was assessed using two-way ANOVA with Tukey's multiple comparison test. Data plotting and statistical analysis were performed using GraphPad Prism 8 (GraphPad Software, San Diego, CA). A value of $P < 0.05$ was considered significant.

Conflict of interest

The authors declare no conflicts of interest.

Author contributions

J.H.C. and I.H. designed and supervised the experiments and analysed the data. J.H.C., S.J.S., H.K. and E.Y.J. wrote the manuscript. E.-J.S. designed a codon-optimized S protein gene. S.J.S. and H.P.D. conducted S antigen expression and purification experiments. H.J. performed the EM experiment. M.R.I.K made the CRT and 3P mutations. H.K., E.Y.J. and M.S.L. conducted the animal experiments, ADE, and ELISPOT. Y.J.L. and J.H.N. performed PRNT. J.H.N. and S.R.K. expressed recombinant proteins and conducted ELISAs.

References

Ai, J., Zhang, H., Zhang, Q., Zhang, Y., Lin, K., Fu, Z., Song, J. *et al*. (2022) Recombinant protein subunit vaccine booster following two-dose inactivated vaccines dramatically enhanced anti-RBD responses and neutralizing titers against SARS-CoV-2 and variants of concern. *Cell Res.* **32**, 103–106.

Aldén, M., Olofsson Falla, F., Yang, D., Barghouth, M., Luan, C., Rasmussen, M. and De Marinis, Y. (2022) Intracellular reverse transcription of Pfizer BioNTech COVID-19 mRNA vaccine BNT162b2 in vitro in human liver cell line. *Curr. Issues Mol. Biol.* **44**, 1115–1126.

Andrews, N., Stowe, J., Kirsebom, F., Toffa, S., Rickeard, T., Gallagher, E., Gower, C. *et al*. (2022) Covid-19 vaccine effectiveness against the omicron (B.1.1.529) variant. *N. Engl. J. Med.* **386**, 1532–1546.

Berger, I. and Schaffitzel, C. (2020) The SARS-CoV-2 spike protein: balancing stability and infectivity. *Cell Res.* **30**, 1059–1060.

Bos, R., Rutten, L., van der Lubbe, J.E.M., Bakkers, M.J.G., Hardenberg, G., Wegmann, F., Zuijdgeest, D. *et al*. (2020) Ad26 vector-based COVID-19 vaccine encoding a prefusion-stabilized SARS-CoV-2 Spike immunogen induces potent humoral and cellular immune responses. *NPJ Vaccines*, **5**, 91.

Brindha, S. and Kuroda, Y. (2022) A multi-disulfide receptor-binding domain (RBD) of the SARS-CoV-2 spike protein expressed in *E. coli* using a SEP-Tag produces antisera interacting with the mammalian cell expressed spike (S1) protein. *Int. J. Mol. Sci.* **23**, 1703.

Buyel, J.F. (2015) Process development strategies in plant molecular farming. *Curr. Pharm. Biotechnol.* **16**, 966–982.

Cai, Y., Zhang, J., Xiao, T., Peng, H., Sterling, S.M., Walsh, R.M., Rawson, S. *et al*. (2020) Distinct conformational states of SARS-CoV-2 spike protein. *Science*, **369**, 1586–1592.

Castells, M.C. and Phillips, E.J. (2021) Maintaining safety with SARS-CoV-2 vaccines. *N. Engl. J. Med.* **384**, 643–649.

Chen, X., Li, R., Pan, Z., Qian, C., Yang, Y., You, R., Zhao, J. *et al*. (2020) Human monoclonal antibodies block the binding of SARS-CoV-2 spike protein to angiotensin converting enzyme 2 receptor. *Cell. Mol. Immunol.* **17**, 647–649.

Cho, J., Lee, Y.J., Kim, J.H., Kim, S.I., Kim, S.S., Choi, B.S. and Choi, J.H. (2020) Antiviral activity of digoxin and ouabain against SARS-CoV-2 infection and its implication for COVID-19. *Sci. Rep.* **10**, 16200.

Cimini, A., Marconi, O., Perretti, G. and Moresi, M. (2014) Novel procedure for lager beer clarification and stabilization using sequential enzymatic, centrifugal, regenerable PVPP and crossflow microfiltration processing. *Food Bioproc. Tech.* **7**, 3156–3165.

ClinicalTrials.gov (2022) *Evaluation of the Safety, Tolerability, and Reactogenicity of the Baiya SARS-CoV-2 Vax 2 Vaccine*. Bethesda, Maryland: U.S. National Library of Medicine.

Corbett, K.S., Edwards, D.K., Leist, S.R., Abiona, O.M., Boyoglu-Barnum, S., Gillespie, R.A., Himansu, S. *et al*. (2020) SARS-CoV-2 mRNA vaccine design enabled by prototype pathogen preparedness. *Nature*, **586**, 567–571.

Daniell, H., Nair, S.K., Esmaeili, N., Wakade, G., Shahid, N., Ganesan, P.K., Islam, M.R. *et al*. (2022) Debulking SARS-CoV-2 in saliva using angiotensin converting enzyme 2 in chewing gum to decrease oral virus transmission and infection. *Mol. Therapy*, **30**, 1966–1978.

D'Aoust, M.A., Couture, M.M., Charland, N., Trepanier, S., Landry, N., Ors, F. and Vezina, L.P. (2010) The production of hemagglutinin-based virus-like particles in plants: a rapid, efficient and safe response to pandemic influenza. *Plant Biotechnol. J.* **8**, 607–619.

Dhama, K., Natesan, S., Iqbal Yatoo, M., Patel, S.K., Tiwari, R., Saxena, S.K. and Harapan, H. (2020) Plant-based vaccines and antibodies to combat COVID-19: current status and prospects. *Hum. Vaccin. Immunother.* **16**, 2913–2920.

Esposito, D., Mehalko, J., Drew, M., Snead, K., Wall, V., Taylor, T., Frank, P. *et al*. (2020) Optimizing high-yield production of SARS-CoV-2 soluble spike trimers for serology assays. *Protein Expr. Purif.* **174**, 105686.

Francis, A.I., Ghany, S., Gilkes, T. and Umakanthan, S. (2022) Review of COVID-19 vaccine subtypes, efficacy and geographical distributions. *Postgrad. Med. J.* **98**, 389–394.

Gobeil, S.M.C., Janowska, K., McDowell, S., Mansouri, K., Parks, R., Manne, K., Stalls, V. *et al*. (2021) D614G mutation alters SARS-CoV-2 spike conformation and enhances protease cleavage at the S1/S2 junction. *Cell Rep.* **34**, 108630.

Grifoni, A., Sidney, J., Vita, R., Peters, B., Crotty, S., Weiskopf, D. and Sette, A. (2021) SARS-CoV-2 human T cell epitopes: adaptive immune response against COVID-19. *Cell Host Microbe*, **29**, 1076–1092.

HealthCanada. (2022) *Health Canada authorizes Medicago COVID-19 vaccine for adults 18 to 64 years of age*.

Heath, W.R. and Carbone, F.R. (2001) Cross-presentation in viral immunity and self-tolerance. *Nat. Rev. Immunol.* **1**, 126–134.

Hogenesch, H. (2012) Mechanism of immunopotentiation and safety of aluminum adjuvants. *Front. Immunol.* **3**, 406.

Hossain, M.G., Tang, Y.D., Akter, S. and Zheng, C. (2022) Roles of the polybasic furin cleavage site of spike protein in SARS-CoV-2 replication, pathogenesis, and host immune responses and vaccination. *J. Med. Virol.* **94**, 1815–1820.

Hsieh, C.-L., Goldsmith, J.A., Schaub, J.M., DiVenere, A.M., Kuo, H.-C., Javanmardi, K., Le, K.C. *et al*. (2020) Structure-based design of prefusion-stabilized SARS-CoV-2 spikes. *Science*, **369**, 1501–1505.

Jackson, C.B., Farzan, M., Chen, B. and Choe, H. (2022) Mechanisms of SARS-CoV-2 entry into cells. *Nat. Rev. Mol. Cell Biol.* **23**, 3–20.

Joffre, O.P., Segura, E., Savina, A. and Amigorena, S. (2012) Cross-presentation by dendritic cells. *Nat. Rev. Immunol.* **12**, 557–569.

Li, T., Zheng, Q., Yu, H., Wu, D., Xue, W., Xiong, H., Huang, X. *et al*. (2020) SARS-CoV-2 spike produced in insect cells elicits high neutralization titres in non-human primates. *Emerg Microbes Infect*, **9**, 2076–2090.

Liu, Y., Dai, L., Feng, X., Gao, R., Zhang, N., Wang, B., Han, J. *et al*. (2021) Fast and long-lasting immune response to S-trimer COVID-19 vaccine adjuvanted by PIKA. *Mol. Biomed.* **2**, 29.

Lu, Y., Welsh, J.P. and Swartz, J.R. (2014) Production and stabilization of the trimeric influenza hemagglutinin stem domain for potentially broadly protective influenza vaccines. *Proc. Natl. Acad. Sci.* **111**, 125–130.

Maharjan, P.M. and Choe, S. (2021) Plant-Based COVID-19 Vaccines: Current Status, Design, and Development Strategies of Candidate Vaccines. *Vaccines (Basel)*, **9**, 992.

Mamedov, T., Musayeva, I., Acsora, R., Gun, N., Gulec, B., Mammadova, G., Cicek, K. *et al*. (2019) Engineering, and production of functionally active human Furin in *N. benthamiana* plant: in vivo post-translational processing of target proteins by Furin in plants. *PLoS One*, **14**, e0213438.

Mamedov, T., Yuksel, D., Ilgin, M., Gurbuzaslan, I., Gulec, B., Mammadova, G., Ozdarendeli, A. *et al*. (2021) Production and characterization of nucleocapsid and RBD cocktail antigens of SARS-CoV-2 in *Nicotiana benthamiana* plant as a vaccine candidate against COVID-19. *Vaccines (Basel)*, **9**, 1337.

Margolin, E., Oh, Y.J., Verbeek, M., Naude, J., Ponndorf, D., Meshcheriakova, Y.A., Peyret, H. *et al*. (2020) Co-expression of human calreticulin significantly improves the production of HIV gp140 and other viral glycoproteins in plants. *Plant Biotechnol. J.* **18**, 2109–2117.

Mittal, A., Manjunath, K., Ranjan, R.K., Kaushik, S., Kumar, S. and Verma, V. (2020) COVID-19 pandemic: insights into structure, function, and hACE2 receptor recognition by SARS-CoV-2. *PLoS Pathog.* **16**, e1008762.

Nemet, I., Kliker, L., Lustig, Y., Zuckerman, N., Erster, O., Cohen, C., Kreiss, Y. *et al*. (2022) Third BNT162b2 vaccination neutralization of SARS-CoV-2 omicron infection. *N. Engl. J. Med.* **386**, 492–494.

Nguyen-Contant, P., Embong, A.K., Kanagaiah, P., Chaves, F.A., Yang, H., Branche, A.R., Topham, D.J. *et al*. (2020) S protein-reactive IgG and memory B cell production after human SARS-CoV-2 infection includes broad reactivity to the S2 subunit. *mBio*, **11**, e01991-20.

Norkunas, K., Harding, R., Dale, J. and Dugdale, B. (2018) Improving agroinfiltration-based transient gene expression in *Nicotiana benthamiana*. *Plant Methods*, **14**, 71.

Oladunni, F.S., Park, J.G., Pino, P.A., Gonzalez, O., Akhter, A., Allue-Guardia, A., Olmo-Fontanez, A. *et al*. (2020) Lethality of SARS-CoV-2 infection in K18 human angiotensin-converting enzyme 2 transgenic mice. *Nat. Commun.* **11**, 6122.

Ord, M., Faustova, I. and Loog, M. (2020) The sequence at Spike S1/S2 site enables cleavage by furin and phospho-regulation in SARS-CoV2 but not in SARS-CoV1 or MERS-CoV. *Sci. Rep.* **10**, 16944.

Pajon, R., Doria-Rose, N.A., Shen, X., Schmidt, S.D., O'Dell, S., McDanal, C., Feng, W. *et al*. (2022) SARS-CoV-2 omicron variant neutralization after mRNA-1273 booster vaccination. *N. Engl. J. Med.* **386**, 1088–1091.

Pallesen, J., Wang, N., Corbett, K.S., Wrapp, D., Kirchdoerfer, R.N., Turner, H.L., Cottrell, C.A. *et al*. (2017) Immunogenicity and structures of a rationally designed prefusion MERS-CoV spike antigen. *Proc. Natl. Acad. Sci.* **114**, E7348–E7357.

Peacock, T.P., Goldhill, D.H., Zhou, J., Baillon, L., Frise, R., Swann, O.C., Kugathasan, R. *et al*. (2021) The furin cleavage site in the SARS-CoV-2 spike protein is required for transmission in ferrets. *Nat. Microbiol.* **6**, 899–909.

Pillet, S., Arunachalam, P.S., Andreani, G., Golden, N., Fontenot, J., Aye, P.P., Roltgen, K. *et al*. (2022) Safety, immunogenicity, and protection provided by unadjuvanted and adjuvanted formulations of a recombinant plant-derived virus-like particle vaccine candidate for COVID-19 in nonhuman primates. *Cell. Mol. Immunol.* **19**, 222–233.

Reed, L.J. and Muench, H. (1938) A simple method of estimating fifty percent endpoints. *Am. J. Hygiene*, **27**, 493–497.

Rossler, A., Riepler, L., Bante, D., von Laer, D. and Kimpel, J. (2022) SARS-CoV-2 omicron variant neutralization in serum from vaccinated and convalescent persons. *N. Engl. J. Med.* **386**, 698–700.

Royal, J.M., Simpson, C.A., McCormick, A.A., Phillips, A., Hume, S., Morton, J., Shepherd, J. *et al*. (2021) Development of a SARS-CoV-2 vaccine candidate using plant-based manufacturing and a tobacco mosaic virus-like nano-particle. *Vaccines (Basel)*, **9**, 1347.

Santiago, F.W., Lambert Emo, K., Fitzgerald, T., Treanor, J.J. and Topham, D.J. (2012) Antigenic and immunogenic properties of recombinant hemagglutinin proteins from H1N1 A/Brisbane/59/07 and B/Florida/04/06 when produced in various protein expression systems. *Vaccine*, **30**, 4606–4616.

Sarah A. Buchan, H.C., Brown, K.A., Austin, P.C., Fell, D.B., Gubbay, J.B., View ORCID Profile, Nasreen, S. *et al*. (2022) *Effectiveness of COVID-19 vaccines against Omicron or Delta infection. medRxiv av*.

Sęczyk, Ł., Świeca, M., Kapusta, I. and Gawlik-Dziki, U. (2019) Protein–phenolic interactions as a factor affecting the physicochemical properties of white bean proteins. *Molecules*, **24**, 408.

Shah, P., Canziani, G.A., Carter, E.P. and Chaiken, I. (2021) The case for S2: the potential benefits of the S2 subunit of the SARS-CoV-2 spike protein as an immunogen in fighting the COVID-19 pandemic. *Front. Immunol.* **12**, 637651.

Shang, W., Yang, Y., Rao, Y. and Rao, X. (2020) The outbreak of SARS-CoV-2 pneumonia calls for viral vaccines. *NPJ Vaccines*, **5**, 18.

Simone I. Richardson, V.S.M., Spencer, H., Manamela, N.P., van der Mescht, M.A., Lambson, B.E., Oosthuysen, B., Ayres, F. *et al*. (2022) SARS-CoV-2 Omicron triggers cross-reactive neutralization and Fc effector functions in previously vaccinated, but not unvaccinated individuals. *Cell Host Microbe*, **30**, 880–886.e4.

Siriwattananon, K., Manopwisedjaroen, S., Shanmugaraj, B., Rattanapisit, K., Phumiamorn, S., Sapsutthipas, S., Trisiriwanich, S. *et al.* (2021) Plant-produced receptor-binding domain of SARS-CoV-2 elicits potent neutralizing responses in mice and non-human primates. *Front. Plant Sci.* **12**, 682953.

Song, S.-J., Diao, H.-P., Moon, B., Yun, A. and Hwang, I. (2022) The B1 domain of streptococcal protein G serves as a multi-functional tag for recombinant protein production in plants. *Front. Plant Sci.* **13**. https://doi.org/10.3389/fpls.2022.878677

Song, S.J., Shin, G.I., Noh, J., Lee, J., Kim, D.H., Ryu, G., Ahn, G. *et al.* (2021) Plant-based, adjuvant-free, potent multivalent vaccines for avian influenza virus via Lactococcus surface display. *J. Integr. Plant Biol.* **63**, 1505–1520.

Tian, J.H., Patel, N., Haupt, R., Zhou, H., Weston, S., Hammond, H., Logue, J. *et al.* (2021) SARS-CoV-2 spike glycoprotein vaccine candidate NVX-CoV2373 immunogenicity in baboons and protection in mice. *Nat. Commun.* **12**, 372.

Tran, T.N.M., May, B.P., Ung, T.T., Nguyen, M.K., Nguyen, T.T.T., Dinh, V.L., Doan, C.C. *et al.* (2021) Preclinical immune response and safety evaluation of the protein subunit vaccine nanocovax for COVID-19. *Front. Immunol.* **12**, 766112.

Vogel, A.B., Kanevsky, I., Che, Y., Swanson, K.A., Muik, A., Vormehr, M., Kranz, L.M. *et al.* (2021) BNT162b vaccines protect rhesus macaques from SARS-CoV-2. *Nature*, **592**, 283–289.

Walls, A.C., Park, Y.J., Tortorici, M.A., Wall, A., McGuire, A.T. and Veesler, D. (2020) Structure, function, and antigenicity of the SARS-CoV-2 spike glycoprotein. *Cell*, **183**, 1735.

Wang, W., Vinocur, B., Shoseyov, O. and Altman, A. (2004) Role of plant heat-shock proteins and molecular chaperones in the abiotic stress response. *Trends Plant Sci.* **9**, 244–252.

Ward, B.J., Gobeil, P., Seguin, A., Atkins, J., Boulay, I., Charbonneau, P.Y., Couture, M. *et al.* (2021) Phase 1 randomized trial of a plant-derived virus-like particle vaccine for COVID-19. *Nat. Med.* **27**, 1071–1078.

Watanabe, Y., Mendonca, L., Allen, E.R., Howe, A., Lee, M., Allen, J.D., Chawla, H. *et al.* (2021) *Native-like SARS-CoV-2 spike glycoprotein expressed by ChAdOx1 nCoV-19/AZD1222 vaccine. bioRxiv: the preprint server for biology*.

Wei, C.-J., Xu, L., Kong, W.-P., Shi, W., Canis, K., Stevens, J., Yang, Z.-Y. *et al.* (2008) Comparative efficacy of neutralizing antibodies elicited by recombinant hemagglutinin proteins from avian H5N1 influenza virus. *J. Virol.* **82**, 6200–6208.

Wilbers, R.H., Westerhof, L.B., van Raaij, D.R., van Adrichem, M., Prakasa, A.D., Lozano-Torres, J.L., Bakker, J. *et al.* (2016) Co-expression of the protease furin in *Nicotiana benthamiana* leads to efficient processing of latent transforming growth factor-beta1 into a biologically active protein. *Plant Biotechnol. J.* **14**, 1695–1704.

Wilken, L.R. and Nikolov, Z.L. (2012) Recovery and purification of plant-made recombinant proteins. *Biotechnol. Adv.* **30**, 419–433.

Wu, S., Zhong, G., Zhang, J., Shuai, L., Zhang, Z., Wen, Z., Wang, B. *et al.* (2020) A single dose of an adenovirus-vectored vaccine provides protection against SARS-CoV-2 challenge. *Nat. Commun.* **11**, 4081.

Xia, S., Zhu, Y., Liu, M., Lan, Q., Xu, W., Wu, Y., Ying, T. *et al.* (2020) Fusion mechanism of 2019-nCoV and fusion inhibitors targeting HR1 domain in spike protein. *Cell. Mol. Immunol.* **17**, 765–767.

Yan, L., Zhang, Y., Ge, J., Zheng, L., Gao, Y., Wang, T., Jia, Z. *et al.* (2020) Architecture of a SARS-CoV-2 mini replication and transcription complex. *Nat. Commun.* **11**, 5874.

Youn, K.-S., Hong, J.-H., Bae, D.-H., Kim, S.-J. and Kim, S.-D. (2004) Effective clarifying process of reconstituted apple juice using membrane filtration with filter-aid pretreatment. *J. Membr. Sci.* **228**, 179–186.

Yuan, M., Wan, Y., Liu, C., Li, Y., Liu, Z., Lin, C. and Chen, J. (2021) Identification and characterization of a monoclonal antibody blocking the SARS-CoV-2 spike protein-ACE2 interaction. *Cell. Mol. Immunol.* **18**, 1562–1564.

Zhang, L., Richards, A., Barrasa, M.I., Hughes, S.H., Young, R.A. and Jaenisch, R. (2021) Reverse-transcribed SARS-CoV-2 RNA can integrate into the genome of cultured human cells and can be expressed in patient-derived tissues. *Proc. Natl. Acad. Sci.* **118**, e2105968118.

Zhao, H., Tan, Z., Wen, X. and Wang, Y. (2017) An improved syringe agroinfiltration protocol to enhance transformation efficiency by combinative use of 5-Azacytidine, ascorbate acid and Tween-20. *Plants*, **6**, 9.

Zhuang, Z., Lai, X., Sun, J., Chen, Z., Zhang, Z., Dai, J., Liu, D. *et al.* (2021) Mapping and role of T cell response in SARS-CoV-2-infected mice. *J. Exp. Med.* **218**, e20202187.

Supporting information

Additional supporting information may be found online in the Supporting Information section at the end of the article.

Figure S1 Optimizing expression of recombinant S protein constructs in *N. benthamiana*.

Figure S2 Expression of recombinant $S2_{ct}$ and $S2_m$ proteins in *N. benthamiana*.

Figure S3 Expression of S_{ct} in the presence of CRT and its purification by Ni^{2+}-NTA.

Figure S4 Pretreatment with PPVP and activated charcoal removes high molecular weight aggregates and the smeared background.

Figure S5 SARS-CoV-2 S1- and S2-specific antibody responses after plant-produced NS_{ct}Vac vaccination of mice.

Figure S6 SARS-CoV-2 S-specific antibody responses after vaccination of Balb/c mice with inactivated virus.

Figure S7 Evaluation of antibody-dependent enhancement (ADE) after NS_{ct}Vac vaccination.

Table S1 The nucleotide sequences of primers used in this study.